Textural Development of AA 5754 Sheet Deformed under In-Plane Biaxial Tension

S.W. BANOVIC, M.A. IADICOLA, and T. FOECKE

Crystallographic texture evolution was quantified as a function of biaxial strain level and strain path for AA5754-O sheet metal in an effort to provide a physical description of grain rotation resulting from in-plane stretching. Samples were incrementally deformed to near-failure in three strain states (equibiaxial, plane strain, and uniaxial modes) with the rolling direction (RD) and transverse direction (TD) of the sheet parallel to the major stress axis for the latter two cases. The macrotextures were measured using X-ray diffraction techniques. Results showed that for a given strain path similar deformation textures developed in the two material sets (RD- and TD-oriented samples), though the evolution of the deformed texture was not homogeneous over the entire strain range. These variations in orientation intensities were related to the feeder components found in the initial texture and the availability of these components to rotate toward the more stable orientations under the particular mode of deformation. The nonuniform texture development of the sheet along different directions appears to contribute to the anisotropic mechanical response of the sheet during stretching as measured in the evolving multiaxial flow surfaces.

DOI: 10.1007/s11661-008-9547-9

I. INTRODUCTION

OVER the past three decades, aluminum alloys have been increasingly used to replace conventional Fe-base components in automotive applications. Their light weight and excellent corrosion properties make them suitable for both internal structural members and outer-body panels. However, some obstacles to widespread use of these alloys exist, which include unfavorable mechanical response (lower forming limit strains compared to Fe-base counterparts, serrated yielding, and yield plateaus), forming defects (wrinkling and tearing), and macroscopic surface imperfections (orange peel and ridging/roping lines).

Another issue restricting their application concerns numerical modeling presently used to determine the appropriate processing parameters of a given alloy for a specific part. The predictions of multiaxial behavior are largely inaccurate as these models are based on extrapolations or predictions from basic uniaxial tension tests.[1] Further, the constitutive equations available for use in the models and the data used to develop them are limited in the strain states measured, the level of strains achieved, and accuracy of the measurement. Recent work by this research group has shown that this barrier is being overcome as multiaxial flow surfaces can be experimentally determined, out to failure of the sheet, using an *in-situ* X-ray diffraction technique.[2,3]

S.W. BANOVIC, M.A. IADICOLA, and T. FOECKE, Materials Research Engineers, are with the Metallurgy Division, Technology Administration, Department of Commerce, National Institute of Standards and Technology, Gaithersburg, MD 20899. Contact e-mail: swbanovic@nist.gov.

Manuscript submitted October 19, 2007.
Article published online May 17, 2008

Typically, in-plane anisotropy is seen in the mechanical response of rolled sheet, with different uniaxial behavior parallel and perpendicular to the rolling direction (Figure 1(a)). These effects are not limited to the uniaxial case, as shown in Iadicola *et al.*[3] for AA5754-O sheet subjected to biaxial in-plane straining. The plane strain (Figure 1(b)) and equibiaxial (Figure 1(c)) stress-strain data show that typically assumed isotropic (von Mises) transverse responses (*i.e.*, half the first principal stress and equal biaxial stress, respectively) do not actually occur. However, it was seen that by comparing contours of equal plastic work (based on work values at specific values of plastic strain in the uniaxial rolling direction) in stress space (Figure 1(d), for 1, 5, 10, and 15 pct plastic strain) that the initial anisotropy decreased above 4 and 7 pct strain, for plane strain and equibiaxial tension, respectively. Barlat and Richmond[4] have shown that this material anisotropy may be a result of the preferred crystallographic orientation in the as-received sheet. Using the Taylor–Bishop–Hill model, materials with strong initial textures of *Goss* $\{011\}\langle 100\rangle$ and *Brass* (*B*) $\{011\}\langle 211\rangle$ components developed flow surfaces similar to that observed early in the deformation process. However, with increasing plastic strain, the distortion along the σ_{TD} direction was further intensified, and did not agree with the experimental results shown in Figure 1(d). One explanation may be that the model used by Barlat and Richmond did not account for the continually evolving texture that is developed in the sheet as deformation progresses and the subsequent effect that this will have on the flow surface.

While the basic understand of texture changes in aluminum sheet during in-plane forming operations have been studied for uniaxial,[5,6] plane strain,[5,7–9]

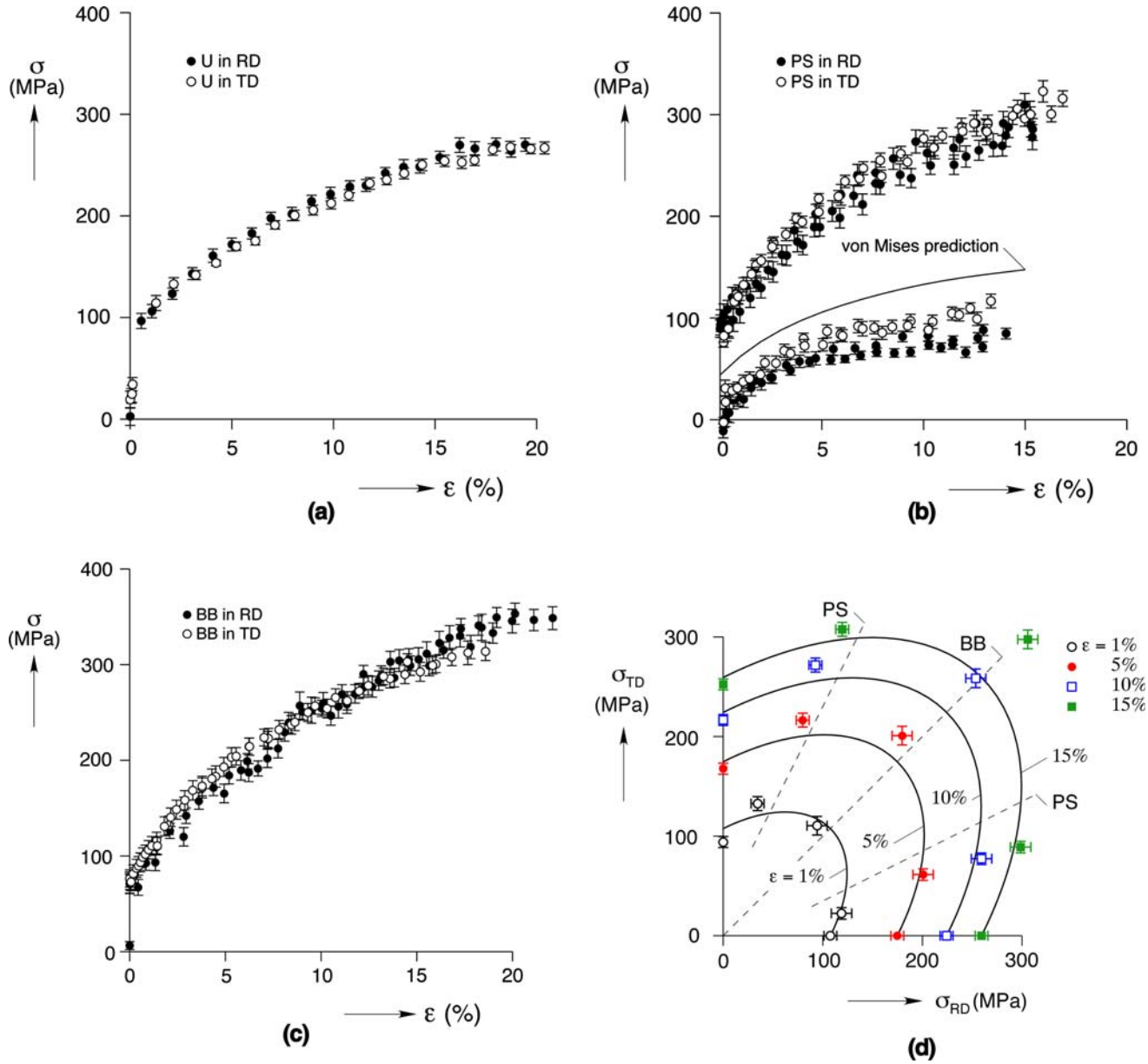

Fig. 1—Multiaxial true stress–true strain data determined through X-ray diffraction[3] for (*a*) uniaxial, (*b*) plane strain, and (*c*) equal biaxial strain. Plane strain stress data for near zero strain direction (and the associated von Mises predicted curve) are plotted using the first principal strain for visibility in (b). (*d*) Derived points of equal plastic work plotted in stress space, with von Mises' isotropic yield loci (solid curves) and isotropic strain paths (dashed lines).

and equibiaxial[5,7–12] stretching, absent in these works was a detailed analysis of the quantitative development of texture modification with incremental plastic straining, particularly in the lower strain regime associated with the sheet metal stamping process. Instead, the greater majority of the work focused on the effect of the initial texture on that of the evolved. Further, only Savoie *et al.*[6] analyzed the crystallographic development along both the rolling direction (RD) and transverse direction (TD) of an aluminum sheet under a single deformation mode (uniaxial). Unfortunately, a corresponding analysis of the mechanical behavior of the materials was not conducted to indicate if the change in sheet orientation, with respect to the major stress axis, had an effect on the properties. Therefore, to help provide a physical description of the evolving yield surfaces throughout the deformation process, investigation of the crystallographic texture development of the material tested by Iadicola *et al.*[3] was initiated. This study characterizes the texture modification as a function of strain level of AA5754-O, which has been deformed along both the sheet RD and TD under three in-plane straining modes (equibiaxial, plane strain, and uniaxial). These results will be used to validate future polycrystal plasticity simulation work.

II. EXPERIMENTAL TECHNIQUES

A. *Materials and Deformation Procedures*

The material used in this investigation was industrially processed AA5754-O sheet, nominally 1-mm thick, with composition given in Table I. Figure 2 shows the as-received microstructure of the commercial sheet material. The grains are relatively equiaxed in the rolling plane (Figure 2(a)) and slightly elongated along the RD (Figure 2(b)). This is indicative of a recrystallized microstructure associated with the O-temper. The nominal grain diameter in the rolling plane was approximately 40 μm. Constituent particles observed in the polished cross section (Figure 2(c)) were well dispersed and identified *via* energy dispersive spectroscopy as primarily Al-Fe-Mn particles.

Samples were cut to appropriate dimensions for testing and deformed in three strain states, indicated by their principal strain ratio (ρ)

$$\rho = \frac{\varepsilon_2}{\varepsilon_1} \qquad [1]$$

where ε_1 and ε_2 are the major and minor strains measured within the plane of the sheet, respectively. Standard test methods were used for uniaxial tension ($\rho = -0.5$) with the rolling direction of the sheet aligned both parallel and perpendicular to the major stress axis. For plane strain ($\rho = 0$) and equibiaxial ($\rho = 1$) tension, a technique based upon the Raghavan[13] modification of the Marciniak in-plane biaxial stretching test[14] was employed; the specialized tooling is a cylindrical ram and binder.[15] Mild steel was used as a washer (driver blank) to prevent failure in the sidewall of the aluminum test sheet; lubricant was applied to those faces in contact with the tooling. The load of the hold-down ring was maintained at approximately 340 kN, so that movement of material inward over the draw bead was restricted while being deformed at a constant central ram speed of 1.0 mm/s. Varying amounts of stretching were obtained by setting the limit control of the central ram to predetermined deflections. The true in-plane strain was determined using a calibrated biaxial extensometer. Similar to uniaxial deformation, plane strain testing was conducted with the sheet RD parallel and perpendicular to the main stress axis. Under all modes, samples were produced approximately every 5 pct true strain to near-failure of the plate, Table II. The through thickness strain, ε_3, was determined through physical measurement of the thickness change. The effective strain, ε_{eff}, for equibiaxial and

Table I. Chemical Composition of As-Received AA5754-O Determined Using ASTM E227

Element	Mass Fraction × 100
Mg	3.75
Mn	0.29
Fe	0.24
Si	0.06
Cr, Cu, Pb, Ni, Sn, Ti, Zn	individually < 0.05
Aluminum	balance

Table II. Strain Levels (Percent) Achieved during In-Plane Deformation*

Nominal Strain Level	ε_1	ε_2	ε_3	ε_{eff}
Equibiaxial				
5	5.1	4.9	−10.6	10.4
10	9.7	9.7	−21.6	21.0
15	13.9	14.0	−27.8	27.9
20	19.9	20.0	−41.2	40.8
Plane strain				
5	4.9	−0.4	−3.5	4.9
10	9.8	−0.7	−8.6	10.7
15	14.2	−0.3	−12.7	14.7
Uniaxial				
5	5.6	−2.3	−3.1	5.6
10	11.6	−4.7	−5.1	11.6
15	16.0	−6.5	−9.5	16.0

*Effective strains for equibiaxial and plane strain modes were calculated using the von Mises criterion.

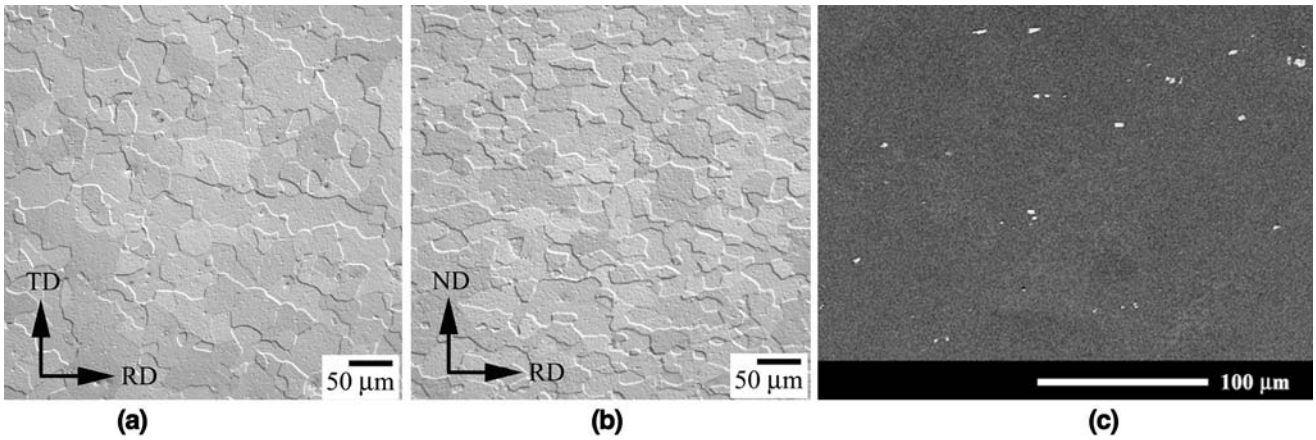

Fig. 2—Microstructures of as-received sheet material: (*a*) and (*b*) differential interference contrast images showing grain size along different directions, and (*c*) SEM showing second phase (white).

plane strain modes was calculated using the von Mises criterion

$$\varepsilon_{\text{eff}} = \frac{\sqrt{2}}{3}\left[(\varepsilon_1 - \varepsilon_2)^2 + (\varepsilon_2 - \varepsilon_3)^2 + (\varepsilon_3 - \varepsilon_1)^2\right]^{1/2} \quad [2]$$

B. *Crystallographic Texture Evaluation*

The macrotextures of the samples were measured using an X-ray diffraction technique on a conventional diffractometer with quarter Eulerian cradle. Samples were illuminated using Cu K_α radiation. In order to eliminate any possible gradients associated with the surface layer, the samples were polished by hand to the midplane of the sheet with a final step of 0.05 μm alumina. An area detector was used to collect three incomplete pole figures {111}, {200}, and {220} with 0 deg $\leq \alpha \leq$ 65 deg. The samples were oscillated over an area of 6.4 cm^2. The data were corrected for background intensity.

For quantitative texture analysis, the three-dimensional orientation distributions (ODs) were calculated from the pole figures using the arbitrary defined cell (ADC) method based upon the work of Pawlik and Pospiech[16] and Li.[17] Orientations were expressed by Euler angles, φ_1, Φ, and φ_2 in Bunge's notation,[18] which relates the cubic crystal frame to the orthotropic sample frame given by the normal direction (ND), the RD, and the TD. To facilitate interpretations of textures, ODs were represented by plotting iso-intensity lines in sections of constant φ_2 through a subset of the Euler angle space with 0 deg $\leq \varphi_1, \Phi, \varphi_2 \leq$ 90 deg. As the textures were weak for the both the initial and deformed materials, recalculated pole figures were derived from the ODs and presented as a substitute of the raw data.

Volume fractions of specific orientations were calculated using the following equation:

$$\frac{dV}{V} = f(g)dg \quad [3]$$

with

$$dg \equiv d(\varphi_1, \Phi, \varphi_2) = 1/8\pi^2 \sin\Phi d\Phi d\varphi_1 d\varphi_2 \quad [4]$$

Integrating all orientations that have their misorientation, with respect to the given ideal orientation, less than the given tolerance yields the volume fraction.

III. CRYSTALLOGRAPHIC TEXTURE DEVELOPMENT

The following convention was used in the presentation of the texture data. Samples were tested with either the rolling direction (RD-oriented material) or transverse direction (TD-oriented material) of the sheet parallel to the major stress axis. For analysis of the {111} pole figures, the major stress axis was aligned parallel to the North-South poles.

A. {111} *Pole Figures*

Figure 3 shows the recalculated pole figures from the as-received materials for both RD- and TD-oriented materials. For the RD sample (Figure 3(a)), the sheet displays a low degree of texture (peak intensity of 2 times random) with a combination of recrystallization (*cube* {001}⟨100⟩, *R* {124}⟨211⟩) and retained deformation (*B* {011}⟨211⟩, *copper* {112}⟨111⟩) components, typical of an O-temper material. Comparing the pole figure from the TD-oriented material (Figure 3b), the two are nearly identical, though rotated 90 deg about the sheet ND. For the TD sample, the cube orientation was also observable due to its four-fold symmetry. Other secondary components were 90 deg rotations about the sheet ND of components noted in the RD-oriented pole figure: rotated (R_{ND})-*R* (approximately {123}⟨341⟩), *P* {011}⟨566⟩ (90 deg rotation of *B* orientation), and R_{ND}-copper{112}⟨110⟩.

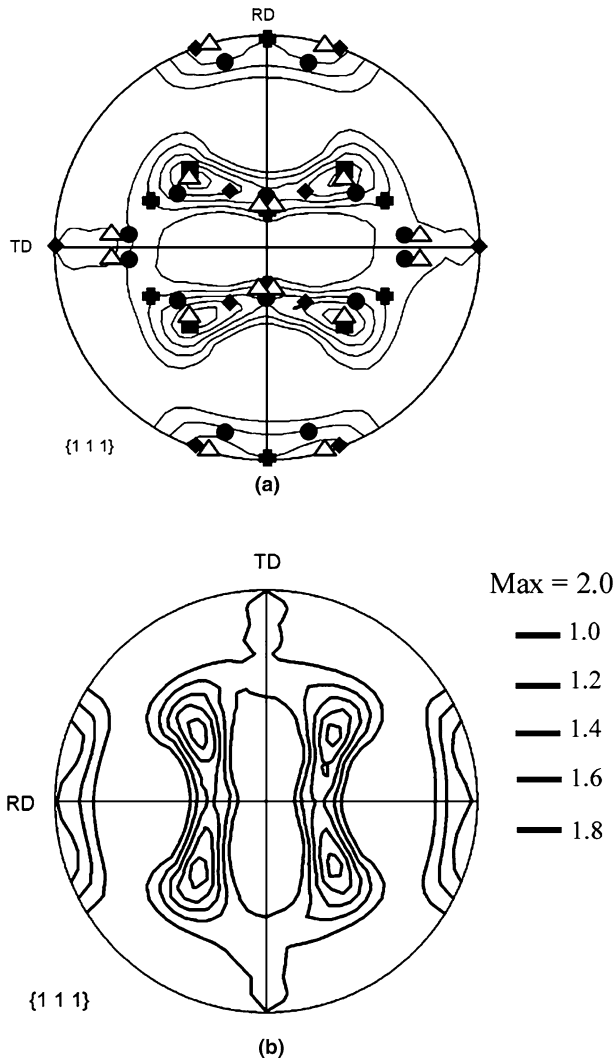

Fig. 3—{111} recalculated pole figures of as-received sheet material: (*a*) RD-oriented material, positions of the ideal orientations are shown (cube ■, *R* ●, Brass ♦, *S* Δ, copper ✚); and (*b*) TD-oriented material.

Figures 4 and 5 show the development of the recalculated {111} pole figures as a function of deformation mode and strain level schematically shown in stress space for the RD- and TD-oriented material, respectively. In both material sets, equibiaxial straining ($\rho = 1$) produced a nonuniform, ringlike pole distribution with maxima readily noted near the *B* (RD-sample set) and *P* (TD-sample set) positions. For plane strain

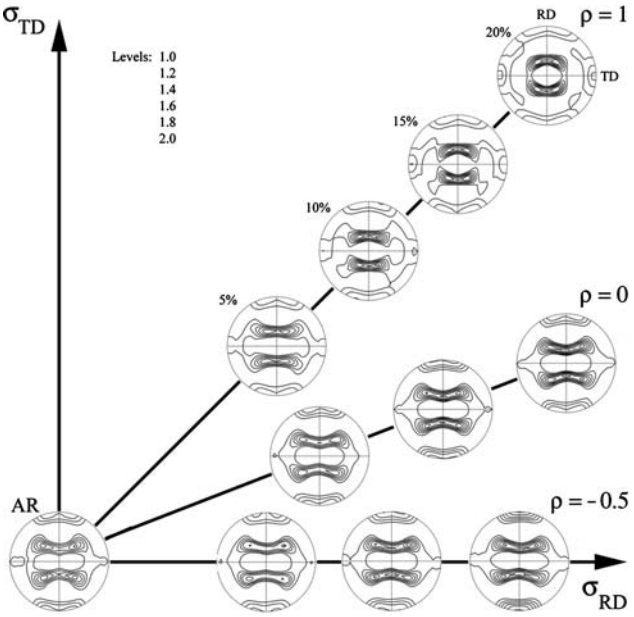

Fig. 4—Change in {111} recalculated pole figure with strain path and strain level for the RD-oriented material where the plane strain and uniaxial samples have their RD parallel to the major stress axis.

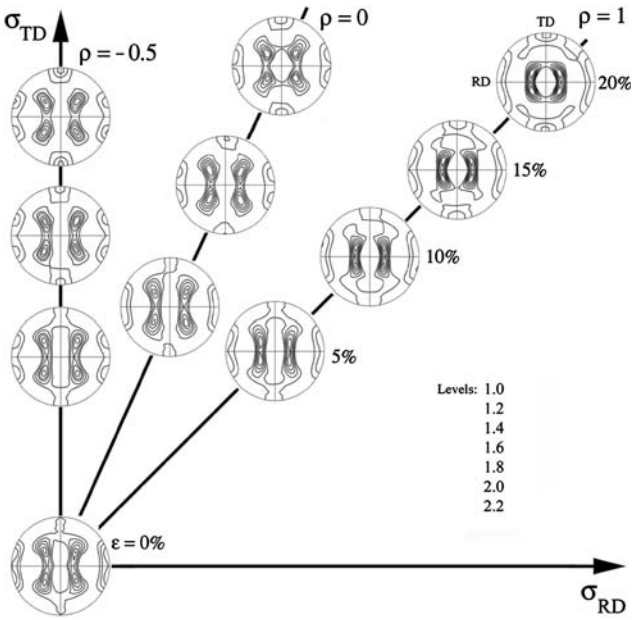

Fig. 5—Change in {111} recalculated pole figure with strain path and strain level for the TD-oriented material where the plane strain and uniaxial samples have their RD perpendicular to the major stress axis.

($\rho = 0$) and uniaxial ($\rho = -0.5$) modes, deformation universally sharpened the majority of as-received texture components, as well as the *S* orientation $\{123\}\langle 634\rangle$, in the RD-oriented material. The TD-oriented material also saw a strengthening of the cube orientation as well as the development of a strong *P* component under plane strain. Both cube and *P* orientations also increased under uniaxial straining, however, preservation of the original texture was stronger in the uniaxial case than in the plane strain condition toward the higher strain level. The degree of texture increased only slightly after the in-plane stretching compared to the as-received material in both RD and TD material sets.

B. *Orientation Distributions*

1. *As-received material*

Recrystallization and retained deformation components are readily observed in the OD of the RD-oriented material (Figure 6(a)). The texture was mainly concentrated around the cube orientation, though it was not exceedingly sharp as spread was observed about all three directions (ND, RD, and TD). Additionally, the *R* component (recrystallization component close to the former rolling texture component, *S*) was present at about one third of the intensity of the cube ($f(g)_{\text{cube}} = 6.0$, $f(g)_R = 1.9$). Retained rolling components (*B* and copper orientations) located in the β fiber were also noted. For the TD-oriented material, the OD was similar, but showed a 90 deg rotation about the ND with maxima observed near the cube and *P* components. Orientation intensity values for these components were similar to their nonrotated counterparts. While no evidence of a retained β fiber, with respect to the tensile axis, was found, components in the R_{ND}-β fiber were observed (*P* and R_{ND}-copper).

2. *Equibiaxial deformation*

Three φ_2 sections ($\varphi_2 = 45$, 60, and 90 deg) were chosen to highlight the evolution of texture across the strain range for each deformation mode. Figure 7 shows these sections for both materials sets strained under equibiaxial conditions. As no distinct major stress axis occurred under this mode of deformation, the material was first analyzed with the X-ray beam perpendicular to the RD of the sheet and then rotated 90 deg about the ND for the TD analysis. In general, deformation resulted in the weakening of the as-received components with strengthening of all orientations along the φ_1 axis at $\Phi = 45$ deg in the $\varphi_2 = 90$ deg section. For the RD-oriented material, a maximum was observed near the *B* orientation, while the *P* component developed for the TD case.

3. *Plane strain deformation*

The φ_2 sections for the samples deformed under plane strain mode are shown in Figure 8. Nearly all orientations found in the as-received RD-oriented material strengthened with deformation with the exception of the copper component (Figure 8(a)). The most substantial change occurred for the cube component, though the spread about this orientation was found to be

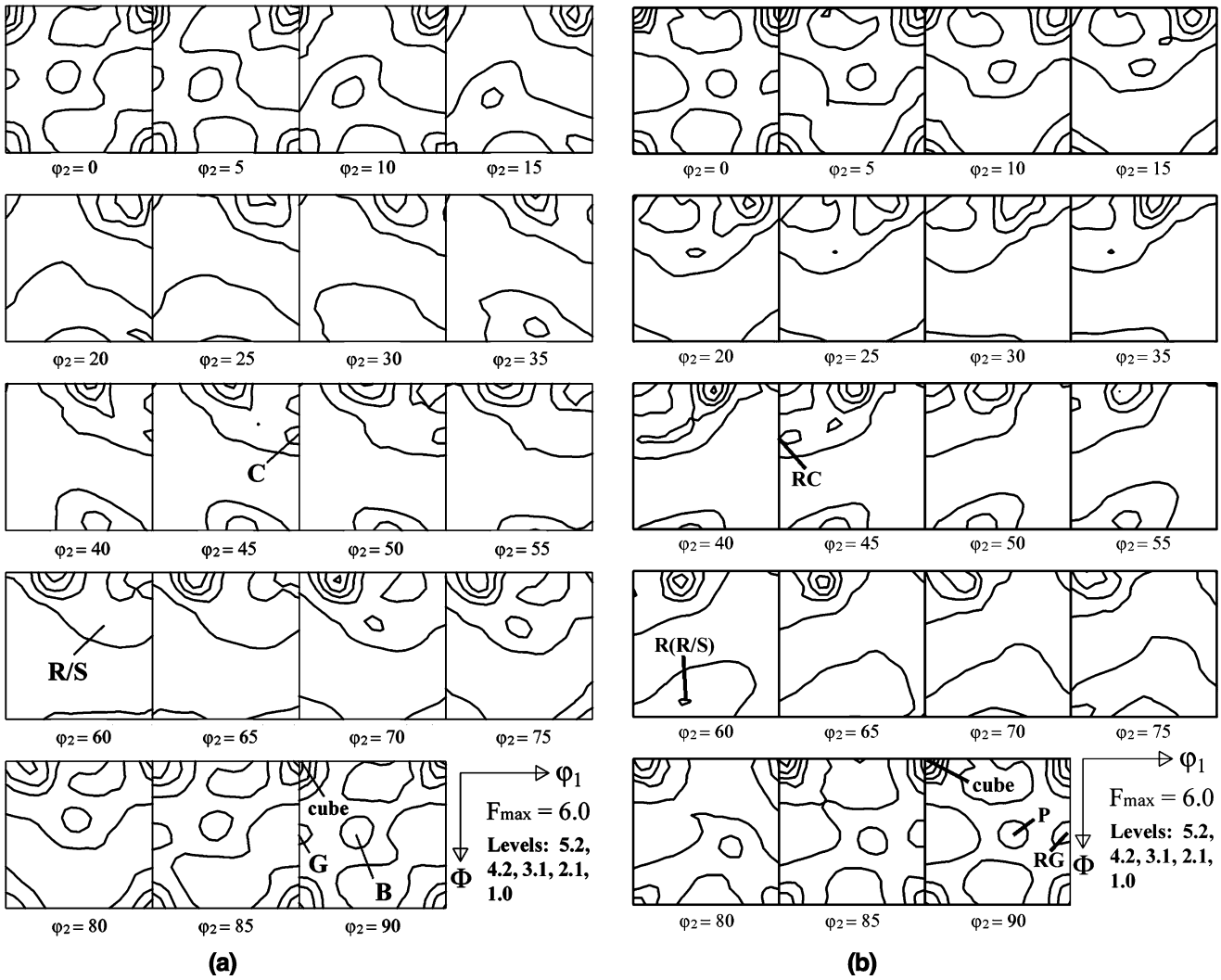

Fig. 6—Orientation distribution for as-received material: (*a*) RD-oriented material with positions of ideal orientations (cube, *R*, Goss, Brass, *S*, copper) and (*b*) TD-oriented material with positions of ideal orientations (cube, R_{ND}-*R*, R_{ND}-Goss, *P*, R_{ND}-*S*, R_{ND}-copper).

inhomogeneous with reduction in the scatter noted along the ND and TD but increased along the RD. Some of the components in the β fiber, specifically *S*, were also observed to increase. Similarly, the TD-oriented material had an overall strengthening of the cube orientation, with an increase in the *P* component (Figure 8(b)). All other orientations decreased.

4. *Uniaxial deformation*

Texture evolution under uniaxial deformation resulted in similar trends as found under plane strain conditions (Figure 9). For the RD-oriented material, the cube component and the majority of orientations found within the β fiber strengthened significantly (Figure 9(a)), while only the cube and *P* orientations increased for the TD case (Figure 9(b)).

C. *Volume Fraction Calculations of Texture Components*

The volume fractions of major texture components were calculated for numerous tolerance angles (ω_0) from 1 deg up to 20 deg from the ideal position. As the trends were consistent at all ω_0, a tolerance angle of 10 deg was chosen to represent the data to ensure that overlap of texture components did not occur during the calculations.

From Figure 6(a), it appears that the cube orientation of the RD-oriented material is the much stronger recrystallization texture component in the as-received material ($f(g)_{\text{cube}} = 6.0, f(g)_R = 1.9$). However, volume fraction calculations indicate that the material contains a higher fraction of *R*-oriented grains (4.5 pct than cube (2.4 pct)), as seen in Table III for the strain level of zero. The difference between orientation intensities and volume fraction results has previously been reported by Engler[19] and is due to the higher symmetry of the cube orientation compared to the *R* orientation. Similarly, the orientation intensities for *B* and copper components in the as-received material are weaker than for cube ($f(g)_B = 2.9$, $f(g)_{\text{copper}} = 2.4$), but volume fraction calculations show that they were nearly equivalent ($B = 2.7$ pct, copper $= 2.2$ pct).

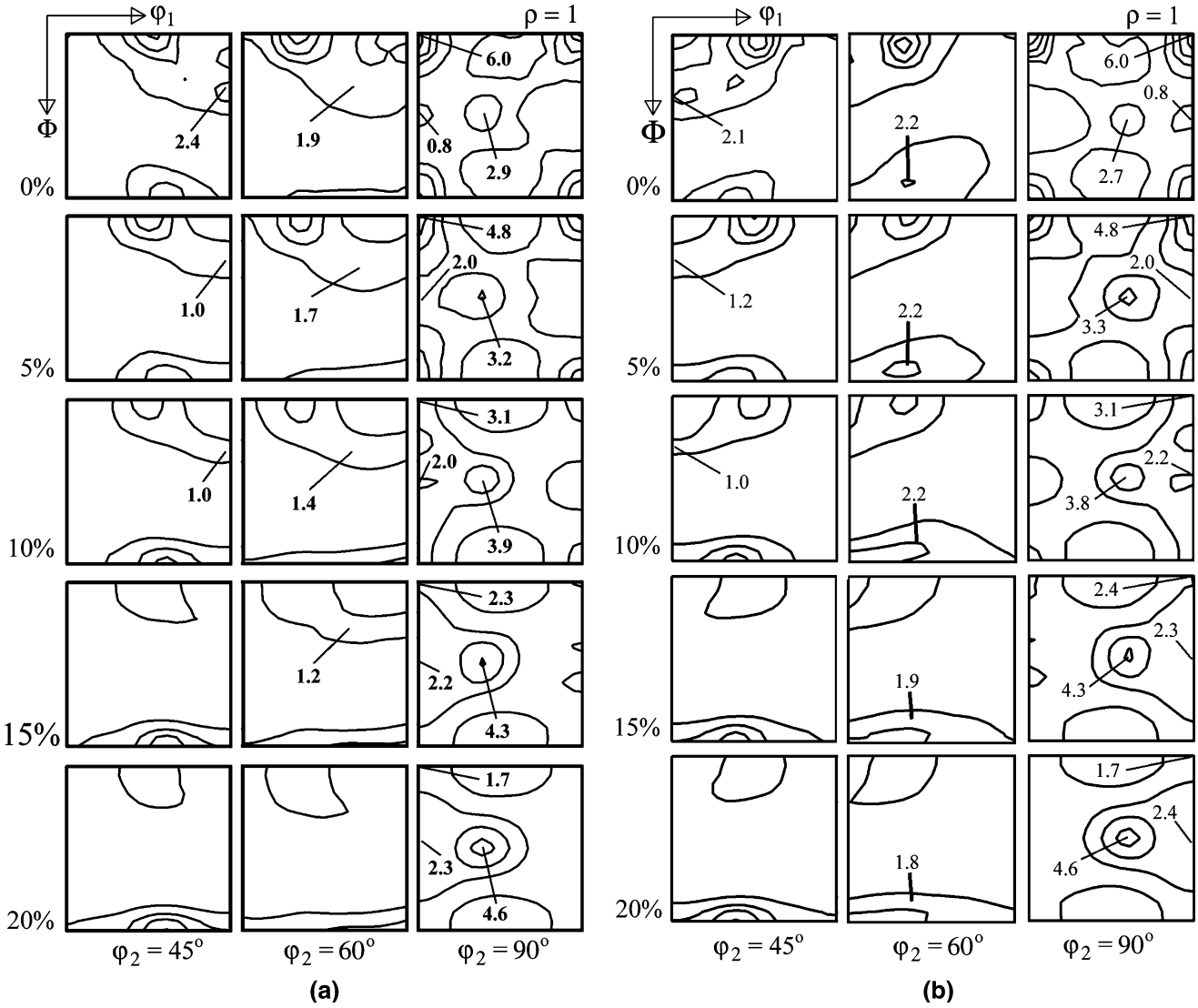

Fig. 7—ϕ_2 sections at given strain levels under equibiaxial conditions ($\rho = 1$): (*a*) RD-oriented material and (*b*) TD-oriented material.

With equibiaxial deformation, the volume fraction of Goss and *B*-oriented grains in the RD-sample set increased, while the major recrystallization and most other retained deformation components decreased (Table III). Volume fraction calculations for plane strain and uniaxial deformation indicated that the most significant increase was for the *S* orientation. All other orientations either increased slightly or stayed approximately the same.

In the TD-oriented as-received material, the cube, *P*, and R_{ND}-copper have similar volume fractions (Table IV). The R_{ND}-*R* position had the highest volume fraction. Equibiaxial deformation resulted in the increase in volume fraction of *P* and R_{ND}-Goss oriented grains; all others decreased. Under plane strain and uniaxial modes, R_{ND}-*R* and R_{ND}-copper decreased and the R_{ND}-Goss component appeared to have little change. While volume fractions of cube and *P* orientations increased for both types of deformation, there was a more notable increase under uniaxial conditions.

IV. DISCUSSION

A. *Crystallographic Texture Evolution*

As the crystallographic anisotropy of the starting aluminum sheet used in this investigation was relatively weak, the deformation-induced textures of the two sample sets for a given straining mode may be expected to be similar. Furthering this argument, one of the major texture components of the sheet is the cube $\{001\}\langle 100\rangle$ orientation, which has fourfold symmetry and should respond similarly when the material is rotated by 90 deg. Therefore, the observed anisotropy of the material during stretch forming is primarily a result of the other texture components that have lower crystallographic symmetry. From the results of this work, it was found that even though the initial texture of the as-received material was weak, it still had a significant effect on the evolved texture as a result of deformation along perpendicular directions for each straining mode.

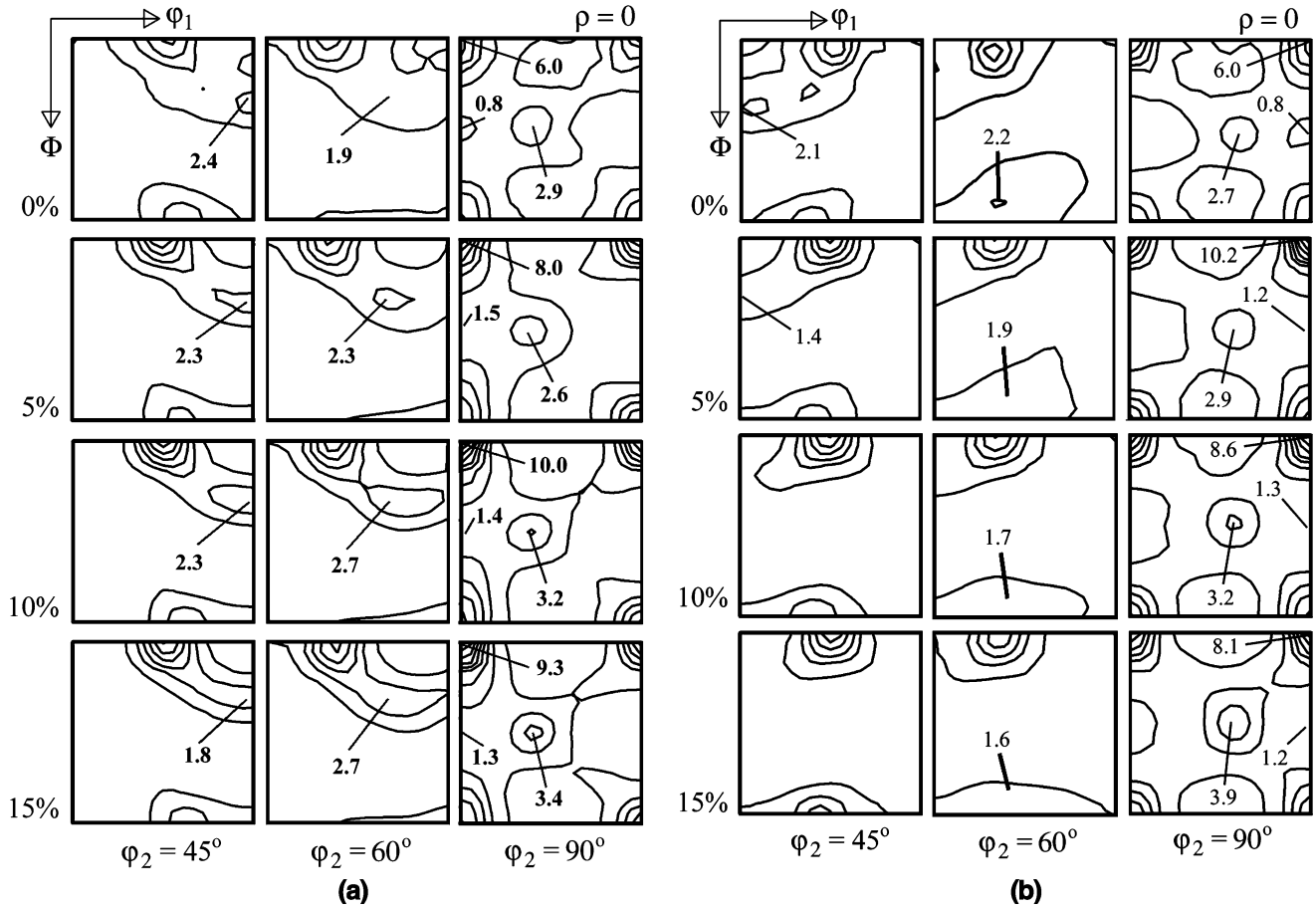

Fig. 8—ϕ_2 sections at given strain levels under plane strain conditions ($\rho = 0$): (*a*) RD-oriented material and (*b*) TD-oriented material.

Metallic sheet materials develop a preferred crystallographic orientation due to their thermomechanical processing. Industrially produced sheet metal typically has a combination of deformation and recrystallization textures subsequent to the rolling and heat treating practices used to obtain an O-temper.[20] For the Al-Mg alloy studied in this investigation, the starting texture of the RD-oriented material contained recrystallization components comprised of cube $\{001\}\langle 100\rangle$ and *R* $\{124\}\langle 211\rangle$ orientations, while the retained rolling textures were copper $\{112\}\langle 111\rangle$ and *B* $\{011\}\langle 211\rangle$.

Of the three strain states evaluated, equibiaxial stretching produced the strongest modification of the initial texture as this mode of deformation resulted in the largest effective strains (Table II). In both sets of samples, grains rotated toward stable orientations located in the $\langle 011\rangle_{ND}$ fiber (along the ϕ_1 axis at $\Phi = 45$ deg, $\phi_2 = 90$ deg), a result previously shown experimentally[5,10,12] and theoretically[7–9,11] on fcc materials. Reviewing these works as a whole indicates that regardless of the alloy composition, starting texture, or technique producing deformation (pure in-plane tension *vs* in-plane tension with out-of-plane bending), texture evolution of fcc materials under equibiaxial conditions is similar. Further, the development of the $\langle 011\rangle_{ND}$ fiber appears to have increased uniformly as a result of the deformation in these previous studies.

From the incremental straining of the sheet during this investigation, the $\langle 011\rangle_{ND}$ fiber development was inhomogeneous (Figure 10). This was a consequence of the different reorientation rates of the individual texture components across the strain range and the availability of unstable feeder components to rotate toward the more stable orientations. At the onset of straining the RD-oriented material, cube grains, and those located between cube and Goss components, rapidly flowed along the Φ-axis toward the Goss position (Figure 6(a)). Physically speaking, this is a rotation about the sheet RD that significantly increased the Goss component during the early stages of deformation. The orientation density near the *B* position also increased in this strain regime, though to a lesser extent than Goss, as grains flowed along the β fiber toward *B*. Both reorientations align the $\langle 110\rangle$ direction of previously unstable grains parallel to the sheet ND, establishing optimum slip conditions along their slip system $\{111\}\langle 110\rangle$ under equibiaxial conditions. With further deformation to 10 pct strain, a significant increase in the orientation density near the *B* position resulted as flow along the β fiber continued to deteriorate the fiber itself (Figure 11(a)). Rotations toward the Goss position slowed considerably as cube-oriented grains have been depleted from earlier deformation. Higher levels of straining resulted in a more homogeneous intensity

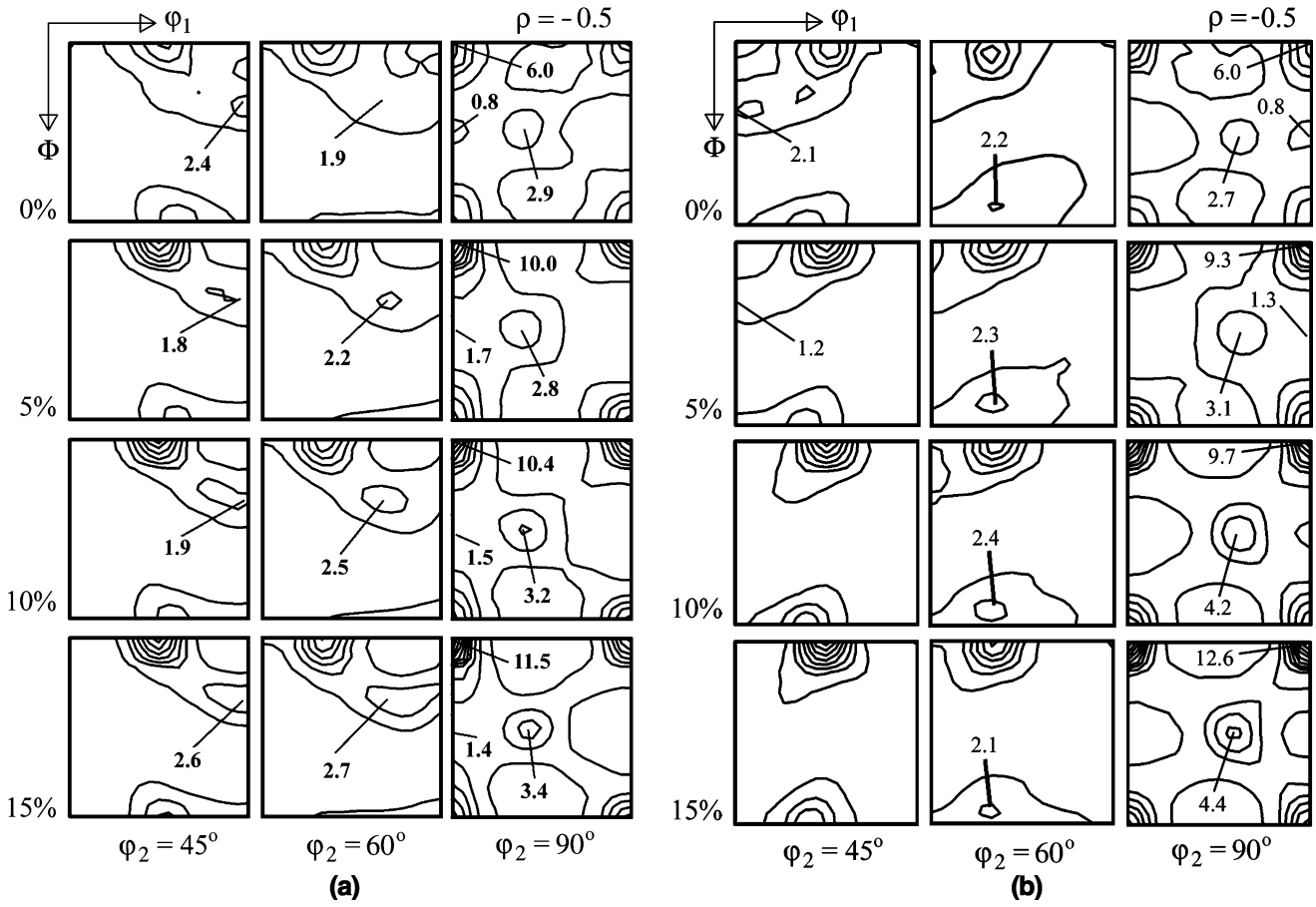

Fig. 9—ϕ_2 sections at given strain levels under uniaxial conditions (ρ = –0.5): (*a*) RD-oriented material and (*b*) TD-oriented material.

Table III. Volume Fraction Calculations of Various Texture Components for RD-Oriented Material (ω_0 = 10 Deg)

Mode	Nominal Strain Level	Cube	Goss	*B*	R/S	Copper
Initial	0	2.4	0.6	2.7	4.5	2.2
Equibiaxial	5	2.0	1.1	3.0	4.0	1.4
	10	1.5	1.1	3.4	3.6	1.3
	15	1.2	1.2	3.9	3.2	1.0
	20	1.0	1.2	4.1	2.9	0.9
Plane strain	5	2.7	0.8	2.7	5.2	2.4
	10	2.9	0.8	2.9	5.9	2.7
	15	2.8	0.8	3.0	5.8	2.2
Uniaxial	5	3.0	0.9	2.7	5.0	2.2
	10	2.8	0.9	2.8	5.5	2.4
	15	2.8	0.8	3.0	5.9	2.9

Table IV. Volume Fraction Calculations of Various Texture Components for TD-Oriented Material (ω_0 = 10 Deg)

Mode	Nominal Strain Level	Cube	R_{ND}-Goss	*P*	R_{ND}-R/S	R_{ND}-Copper
Initial	0	2.4	0.6	2.7	4.9	2.2
Equibiaxial	5	2.0	1.0	3.1	4.0	1.4
	10	1.5	1.1	3.4	3.6	1.3
	15	1.2	1.1	3.9	3.2	1.0
	20	1.0	1.2	4.1	2.8	0.9
Plane strain	5	2.9	0.7	2.7	4.2	1.7
	10	2.8	0.7	3.0	3.6	1.1
	15	2.7	0.7	3.3	3.1	1.0
Uniaxial	5	3.1	0.7	2.9	4.6	1.5
	10	3.1	0.6	3.7	4.3	1.2
	15	3.4	0.5	4.0	4.2	1.1

increase along the entire length of the $\langle 011 \rangle_{ND}$ fiber as unstable grains from across the orientation space continue to flow toward the fiber. The flux of orientations in this manner gives the general result of a uniformly strengthened $\langle 011 \rangle_{ND}$ fiber compared to the as-received texture.

As no distinct major stress axis occurs under equibiaxial deformation, a similar trend was observed for the TD-oriented material, with similar rotations with respect to the sample coordinate system. For this sample set, the starting material displayed the cube component and 90 deg rotations about the sheet ND of those orientations observed for the RD-oriented material. Upon straining, rotations around the sheet RD lead to strengthening of the R_{ND}-Goss component initially, with additional deformation strengthening $\langle 011 \rangle_{ND}$ fiber and, in particular, the *P* orientation $\{011\}\langle 566 \rangle$.

The dissimilar maxima that developed in the two data sets (*e.g.*, development of the strong *B vs P* orientations)

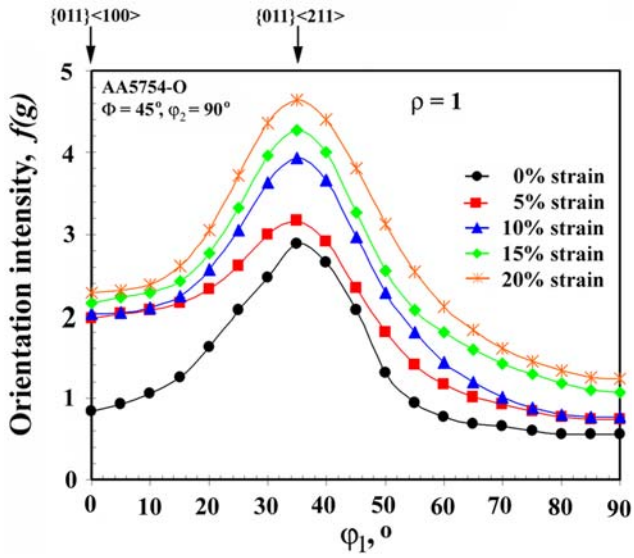

Fig. 10—Orientation intensity plot of $\langle 011 \rangle_{ND}$ fiber under equibiaxial straining conditions for RD-oriented material. Ideal positions for Goss $\{011\}\langle 100 \rangle$ and Brass $\{011\}\langle 211 \rangle$ are indicated.

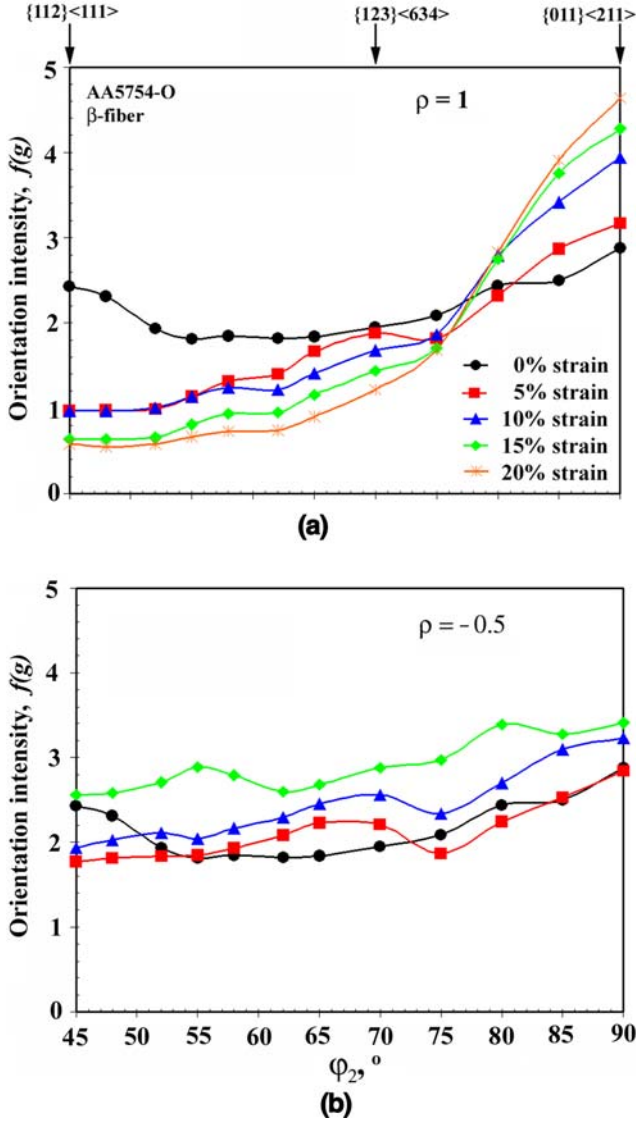

Fig. 11—Orientation intensity plots of β fiber under various straining conditions for RD-oriented material. Ideal positions for copper $\{112\}\langle 111 \rangle$, S $\{123\}\langle 634 \rangle$, and Brass $\{011\}\langle 211 \rangle$ are indicated: (*a*) equibiaxial and (*b*) uniaxial.

were dictated solely by the presence or absence of texture components found in the as-received sheet and not related to stability considerations of the individual components. In an isotropic material, "feeder" components (*i.e.*, those in the β fiber or cube) would be homogeneously distributed at all inclinations with respect to the sheet RD. Under pure equibiaxial stress conditions where no major stress axis exists, maxima would not develop in the $\langle 011 \rangle_{ND}$ fiber as the fiber would strengthen uniformly regardless of crystal direction. This development was modeled by Zhou and Neale[8] using a rate-sensitive crystal plasticity model together with full Taylor constraint theory indicating that any orientation with an $\langle 011 \rangle$ parallel to the sheet ND is stable under equibiaxial conditions. However, as components populated the retained β fiber for the as-received material of the RD-sample set, the B orientation was strengthened due to rotations through the β fiber that feed this particular texture component in the $\langle 011 \rangle_{ND}$ fiber. For the TD-oriented material, feeder components within the β fiber were not observed in the as-received texture (Figure 5(b)), resulting in no grains available to rotate along the fiber toward the B component during deformation. As a result, the B component was not observed to develop. Instead, the P orientation was strengthened through rotations of orientations in the R_{ND}-β fiber present in the TD-as-received material. Thus, while the initial texture would be considered weak, the difference in starting components, such as those in the retained β fiber, was enough to result in dissimilarly evolved textures along the two straining directions under equibiaxial straining, with the strength of the components related to the level of plastic deformation.

Under plane strain and uniaxial stretching, deformation of the material was significantly less than in the equibiaxial case, ε_{eff}, of Table II. When compared to balanced biaxial stretching, with two equal orthogonal in-plane strains, the thickness strain to maintain constant volume in uniaxial or plane strain tension is on the order of one half as large. Concurrently, a less dramatic change was observed in the evolved texture from the as-received material.

In general, significant sharpening of the major starting texture components was observed in both sets of samples, with the additional development of the deformation component S $\{123\}\langle 634 \rangle$ in the RD-oriented material, under both modes of deformation. For the RD-oriented material, straining favored the formation of $\langle 100 \rangle$ fiber parallel to the major stress axis (occupation along the Φ-axis at $\phi_1 = 0$ deg in the $\phi_2 = 90$ deg section in Figures 8(a) and 9(a)) and, to a lesser extent, $\langle 111 \rangle$ fiber parallel to the major stress axis. Alignment of the grains in this manner is in agreement with previous works[5,6,21] that show the $\langle 110 \rangle$ direction as being

unstable under these deformation modes, with grain flux toward the other two directions. However, strengthening in the ⟨100⟩ direction appears to be greater for both cases. This can be attributed to the relative distribution of orientations in the initial texture as the starting material of this work is favored toward the ⟨100⟩. Wassermann and Grewen have previously shown a similar influence by the starting texture on that of the evolved.[22] Further, development of a ⟨100⟩ fiber parallel to the major stress axis attempts to maximize the resolved shear stress experienced by the four slip planes of the crystal. The maximum resolved shear stress occurs when the {111} planes are inclined at 45 deg to the tensile axis. For grains with their ⟨100⟩ parallel to the tensile axis, all four {111} slip planes are at 35.3 deg, very near the position of maximum stress. The TD-sample sets also saw a significant increase in the cube position, but did not have a similar spread about the tensile axis (Figure 9(b)). Instead, a strong *P* component emerged increasing the orientations with ⟨111⟩ or near ⟨111⟩ parallel to the major stress axis.

The influence of the starting texture on the evolved texture can be observed when comparing the results obtained between the two data sets. Again, if the material was isotropic, the texture development observed along the RD and TD would be similar. However, the RD-oriented material showed an increase for the *S* {123}⟨634⟩ orientation and other components in the β fiber (Figure 11(b)), whereas the β fiber did not develop for the TD-oriented material. Similar to the equibiaxial case, this was again due to the lack of feeder components of the TD-oriented material in and around the β fiber that would strengthen these texture components during deformation. As orientations in the R_{ND}-β fiber were observed in the starting texture, development of the *P* orientation was seen in the evolved texture due to rotation and flow of the retained deformation components (R_{ND}-*R* and R_{ND}-copper) in the as-received material.

Savoie *et al.*[6] also performed uniaxial experiments with the tensile axis parallel to both the sheet RD and TD of an experimental 5XXX series alloy. Analysis of RD-oriented material showed strengthening of the cube {001}⟨100⟩, *S* {113}⟨574⟩, *P* {011}⟨111⟩, and Goss {011}⟨100⟩ components observed in the as-received texture. Comparable to the results of this work, they also showed that similar textures developed for the TD-oriented material. However, while fibers consisting of ⟨111⟩ and ⟨100⟩ parallel to the tensile axis evolved, the *R* and Goss orientations were weak or missing in the deformation texture as grains oriented near these components were not observed in the starting texture of the TD-oriented material. Based upon the results of Savioe *et al.*, as well as the results of this present study, it can also be concluded that texture development of a weakly textured sheet is anisotropic under plane strain and uniaxial straining.

B. *Influence of Texture on Mechanical Behavior*

The mechanical response of the sheet to a given imposed strain state will be dictated by the aggregate plastic behavior of the grains in the polycrystal. The initial yield stress will be controlled in part by the initial texture, and the hardening behavior in part by how the texture evolves with increasing multiaxial plastic strain. With a dataset that includes both the evolution of the yield surface with strain and the corresponding texture evolution, it can be determined what, if any, characteristics of the multiaxial stress-strain behavior can be explained by the developing crystallographic texture. A complete treatment using a Taylor-type analysis is ongoing, but some characteristics of the flow behavior can be modeled by comparing the experimental results to the numerical yield surface predictions of Barlat and Richmond[4] of idealized textured microstructures.

Barlat and Richmond calculated flow surfaces of fcc rolled sheets containing grains having 50 pct of one of the specified crystallographic orientations (copper, *B*, *S*, cube, and Goss) with the remainder uniformly distributed over the remaining orientations. An isotropic case was also considered. The yield surfaces were then plotted in stress space after being normalized on the uniaxial yield stress in the rolling direction for each texture component. According to these calculations, the isotropic case, cube and *S* textured sheets showed yield surfaces that were symmetric about the 45 deg (*i.e.*, identical yield behavior parallel and perpendicular to the rolling direction), where cube had a slightly larger flow stress in plane strain. Essentially all three orientations behaved very similarly. Compared to the isotropic results, the sheet containing the copper orientations exhibited a strength decrease for plane strain in the transverse direction and an increase for plane strain in the longitudinal direction. The two remaining sheets, with orientations of *B* and Goss, show very asymmetric yield surfaces, with Goss producing a 50 pct increase in plane strain yield stress in the transverse direction compared to the longitudinal. The values of the respective normalized flow stresses measured from the plots in Reference 4 are given in Table V.

A reasonable first approximation of the behavior of the sheets in the present study is a linear combination of the flow stresses predicted in Reference 4, weighted by the volume fraction of grains with each crystallographic orientation at each multiaxial strain level (Table III). This in effect treats the sheet as a composite made up of a matrix of grains, which average to relatively isotropic properties and a dispersion of grains, each with one of the specified crystallographic orientations, of the appropriate measured volume fraction. The trend of these values can then be compared to the experimentally determined flow stresses.

The values calculated in Reference 4 were each normalized to the uniaxial flow stress of that particular texture component. In order to combine them into a composite flow stress, they must be renormalized to a common flow stress. This is accomplished by calculating the uniaxial RD Schmid factors for the various possible slip planes for the texture components of interest, and dividing each normalized strength by its corresponding maximum uniaxial Schmid factor (Table V). While this does not give an absolute value of the flow stress that can be directly compared to experiments, it gives relative values that will be used to compare to trends in the data.

Table V. Values of Normalized Yield Stresses from Reference 4*

Direction	Cube	Goss	B	S	Copper	Isotropic
BB-RD	1.00	1.00	1.10	1.00	0.90	1.00
BB-TD	1.00	1.40	1.20	1.00	0.85	1.00
PS-RD	1.10	1.10	1.10	1.10	1.10	1.10
PS-RDM	0.50	0.60	0.50	0.45	0.40	0.50
PS-TD	1.10	1.50	1.20	1.10	0.95	1.10
PS-TDM	0.50	0.75	0.75	0.50	0.30	0.50
U-RD	1.00	1.00	1.00	1.00	1.00	1.00
U-TD	1.00	1.40	1.10	0.95	0.90	1.00
Schmid factor	0.41	0.41	0.41	0.43	0.27	0.40

*Note "M" denotes plane strain minor stress. Values are for theoretical mixtures of 50 pct isotropic and 50 pct respective texture component. Also shown are the maximum Schmid factors calculated for each orientation in uniaxial tension in the RD.

The composite flow stress for a given strain level and state due to the texture is then given by

$$\bar{\sigma}_{YS} = \sum \bar{\sigma}_{BR} * \frac{1}{SF_{RD,\text{Uniaxial}}} * V_f \qquad [5]$$

summed over all texture components including the isotropic matrix, where $\bar{\sigma}_{BR}$ is the Barlat–Richmond predicted multiaxial yield stress, $SF_{RD,\text{Uniaxial}}$ is the maximum Schmid factor for the slip planes of the texture component in uniaxial tension in the rolling direction, and V_f is the measured volume fraction of each texture component. For biaxial strain states (plane strain, PS and equibiaxial, BB), the ratio of the stress in the transverse direction to that in the rolling direction is calculated, and compared to ideal isotropic results from von Mises yield theory, the fcc isotropic case of Barlat and Richmond,[4] and to the experimental observations of this study (for nominally 5 pct strain). Note: For the random texture, the $SF_{RD,\text{Uniaxial}}$ value is not known, but the values of $V_{f,\text{Random}}$ (the remainder of the volume) and $\bar{\sigma}_{BR}$ (symmetric in RD and TD) are known. The calculated ratios reported in Table VI neglect this term (*i.e.*, $V_{f,\text{Random}} = 0$). The other extreme would be to calculate the ratio values for $V_{f,\text{Random}} = 1$ from Table V (where the *SF* values being the same will divide to 1), which would result in the values labeled as "Isotropic case."

In Table VI, the experimental ratios (calculated from Figure 1(d)) are distinctly different from the von Mises' isotropic predictions for the three strain states shown, but the isotropic case from Barlat and Richmond deviate from these values for plane strain in the direction of the experimental results. The calculated values using the previous equation tend to move the ratio values closer to the experimental values for all three biaxial strain states. This would suggest that a polycrystal model would be able to capture some of the changes in mechanical behavior if the texture changes are included (especially for the specific components considered here), and since the mechanical behavior and texture both change with increased deformation, the model used must include and properly predict the texture evolution. Additionally, the model will have to account for other factors, such as the work hardening characteristics of the various texture components and grain morphology. This might explain the remaining difference between numerical and experimental results. Therefore, modeling efforts are currently underway using a Taylor-type analysis that will admit texture evolution and work hardening, unlike the Taylor–Bishop–Hill model used by Barlat and Richmond.[4]

Table VI. Values of Yield Stress Ratios (Transverse over Rolling Direction) after 5 Pct Multiaxial Prestrain

	PS-TD	PS-RD	BB
Von Mises' isotropic	2.00	0.50	1.00
fcc isotropic case[4]	2.20	0.45	1.00
Calculated (Eq. [5])	2.27	0.43	1.01
Experimental (Fig. 1(d))	2.71	0.31	1.12

V. CONCLUSIONS

The presented work provides the physical description of texture evolution of a solution-strengthened Al-Mg alloy whose flow surfaces were previously measured.[5] From the results, it was observed that the change in texture with in-plane stretching is considerably less significant compared to other deformation processes of aluminum alloys where through-thickness strains are well in excess of unity (rolling, equal channel extrusion). However, investigation of this lower strain regime is necessary, as these strains are on the same order as those observed during stamping operations. Further, as sheet materials are rarely isotropic and deformation of sheet metal typically does not occur exclusively along one direction, it is necessary to investigate the mechanical properties and subsequently evolved texture along numerous directions to fully understand the behavior of the material. From the results of this work, it was found that similar textures developed in the two material sets (RD- and TD-oriented samples) under each mode of deformation, however, the strength of specific orientations depended upon the amount of deformation and intensity of components in the as-received material. The differences were primarily related to the flow of retained deformation components located in the β fiber during straining of the sheet; the β fiber was observed for the RD-oriented material but not for the TD-oriented material. This nonuniform texture development of the deformed sheet appears to contribute to the anisotropic mechanical response of the sheet during stretching.

REFERENCES

1. A. Ofenheimer, D. Kitting, M.A. Iadicola, and T. Foecke: *Proc. Soc. Autom. Eng.*, SP-2103, 2007, No. 1, in press.
2. T. Foecke, M.A. Iadicola, A. Lin, and S.W. Banovic: *Metall. Mater. Trans. A*, 2007, vol. 38A, pp. 306–13.

3. M.A. Iadicola, T. Foecke, and S.W. Banovic: *Int. J. Plasticity*, in press.
4. F. Barlat and O. Richmond: *Mater. Sci. Eng.*, 1987, vol. 95 (1), pp. 15–29.
5. J.C. Starczan, D. Ruer, and R. Baro: *Proc. ICOTOM 6*, Iron and Steel Institute, Tokyo, 1981, pp. 308–16.
6. J. Savoie, Y. Zhou, J.J. Jonas, and S.R. Macewen: *Acta Mater.*, 1996, vol. 44 (2), pp. 587–605.
7. Y. Zhou and K.W. Neale: *Text. Microstruct.*, 1993, vol. 22, pp. 87–111.
8. Y. Zhou and K.W. Neale: *Mater. Sci. Forum*, 1994, vols. 157–162, pp. 873–78.
9. Y. Zhou and K.W. Neale: *Acta Mater.*, 1994, vol. 42 (6), pp. 2175–2189.
10. S. Kohara: *Proc. 6th Int. Conf. Textures of Materials*, Iron and Steel Institute of Japan, Tokyo, 1981, pp. 300–07.
11. L.S. Tóth, J. Hirsch, and P. Van Houtte: *Int. J. Mech. Sci.*, 1996, vol. 38 (10), pp. 1117–26.
12. S.W. Banovic and T. Foecke: *Metall. Mater. Trans. A*, 2003, vol. 34A, pp. 657–71.
13. K.S. Raghavan: *Metall. Mater. Trans. A*, 1995, vol. 26A, pp. 2075–20.
14. Z. Marciniak and K. Kuczynski: *Int. J. Mech. Sci.*, 1967, vol. 9, pp. 609–20.
15. T. Foecke, S.W. Banovic, and R.J. Fields: *JOM*, 2001, vol. 53 (2), pp. 27–30.
16. K. Pawlik and J. Pospiech: in *Theoretical Methods of Texture Analysis*, H.J. Bunge, ed., DGM Metallurgy Information Adenauerallee, Oberursel, Germany, 1987, p. 127.
17. Li Hualong: Ph.D. Thesis, McGill University, Montreal, 1999.
18. H.J. Bunge: *Texture Analysis in Materials Science-Mathematical Methods*, Butterworth and Company, London, 1982, pp. 1–41.
19. O. Engler: *Metall. Mater. Trans. A*, 1999, vol. 30A, pp. 1517–27.
20. H. Jin and D.J. Lloyd: *Mater. Sci. Eng. A*, 2005, vol. 399, pp. 358–67.
21. G.Y. Chin, W.L. Mammel, and M.T. Dolan: *Trans. TMS-AIME*, 1967, vol. 239, pp. 1854–55.
22. G. Wassermann and J. Grewen: *Texturen Metallischer Werkstoffe*, Springer, Berlin, 1962, p. 57.